Space-charge recombination currents and their influence on the dc current gain of AlGaAs/GaAs *Pnp* heterojunction bipolar transistors

S. Ekbote, M. Cahay,[a] and K. Roenker
Department of Electrical and Computer Engineering and Computer Science, University of Cincinnati, Cincinnati, Ohio 45221

T. Kumar
Dallas Semiconductor, Dallas, Texas 75244

(Received 22 July 1999; accepted for publication 10 September 1999)

The effects of Shockley–Read–Hall, Auger, radiative, and intrinsic surface base recombination processes in the emitter-base space-charge region on the current gain of *Pnp* AlGaAs/GaAs heterojunction bipolar transistors are analyzed. At low forward emitter-base bias, the current gain of a typical *Pnp* AlGaAs/GaAs heterojunction bipolar transistor is shown to be reduced substantially below its value calculated while neglecting recombination currents in the emitter-base space-charge region. Excellent agreement between theory and experiment is found for the current gain variation versus collector current density for a *Pnp* device recently reported by Slater *et al.* [IEEE Electron Device Lett. **15**, 91 (1994)]. © *1999 American Institute of Physics.* [S0021-8979(99)03324-1]

I. INTRODUCTION

The development of *Pnp* GaAs-based transistors for use in complementary heterojunction bipolar transistor technology in the AlGaAs/GaAs materials system has attracted increased interest over the last few years.[1–7] For example, Enquist *et al.*[1] have demonstrated *Pnp* transistors with gain up to 300 at 1.5×10^4 A/cm^2 with unity current gain frequency f_T of 21 GHz and maximum frequency of oscillation $f_{\max}$ of 23 GHz. Based on these devices, they have demonstrated a low-power, high-speed, complementary heterojunction bipolar transistor (HBT)-based, integrated injection logic (I^2L) with 65 ps and 13 mW per gate for a speed-power product of 850 fJ.[1] Hill *et al.*[8,9] and Liu *et al.*[10,11] have obtained *Pnps* with current gain of 200, an f_T of 23 GHz and an $f_{\max}$ of 40 GHz and demonstrated a push-pull power amplifier at 10 GHz with an output power of 500 mW with 6 dB gain and a 41.8% power added efficiency.

So far, there has been only a few reports on the modeling of AlGaAs/GaAs *Pnp* HBTs.[12–14] Hutchby[12] has theoretically estimated that a *Pnp* AlGaAs/GaAs HBT to be capable of an f_T of 31 GHz and an $f_{\max}$ of 94 GHz for a 1 μm wide emitter, parameter values comparable to the *Npn* HBT. While the *Pnp* device's structure needs to be optimized for each material system, this projection of *Pnp* performance comparable to that of the *Npn* has been reinforced by the analysis of Sunderland and Dapkus[13] as well as that of Yuan.[14] Hereafter, we develop an analytical model of AlGaAs/GaAs *Pnp* HBTs to be used by device designers prior to actual device fabrication. Our model includes the effects of the recombination currents in the quasi-neutral base and in the emitter-base space-charge region. Similar models have been developed recently for *Npn* HBTs[15,16] and used to investigate which component of the base current dominates and leads to degradation of the dc current gain β.

Our approach follows the analysis of Searles and Pulfrey for AlGaAs/GaAs *Npn* HBTs.[16] They show that, in order to calculate accurately the dc current gain of *Npn* HBTs, one must include the bias dependence of the electron quasi-Fermi level splitting at the emitter-base heterojunction.[16,17] Similarly, the presence of an abrupt emitter-base heterojunction in a *Pnp* HBT leads to a splitting of the hole quasi-Fermi level ΔE_{fp} at the heterointerface as shown in Fig. 1.[18] In this article, we follow Searles and Pulfrey and calculate ΔE_{fp} using a balancing of the thermionic/tunneling current $J_{\rm ThT}$ crossing the abrupt junction, with the following current components in the base: (1) the (intrinsic base) surface recombination current due to traps at the emitter-base junction ($J_{\rm BS}$), (2) the space-charge recombination current on the base side of the space-charge region ($J_{{\rm SCR},B}$), (3) the neutral base recombination current ($J_{\rm NB}$), and (4) the hole flow producing the collector current (J_C), i.e.,

$$J_{\rm ThT}=J_{\rm BS}+J_{{\rm SCR},B}+J_{\rm NB}+J_C\rightarrow\Delta E_{fp}\,. \tag{1}$$

The base current is calculated by including the effects of recombination in the quasi-neutral base ($J_{\rm NB}$) and the various recombination currents in the emitter-base space-charge region [Shockley–Read–Hall (SRH), Auger ($J_{\rm Aug}$), radiative ($J_{\rm rad}$), and intrinsic base surface currents], i.e.,

$$J_B=J_{\rm SCR}+J_{\rm NB}\,, \tag{2}$$

where

$$J_{\rm SCR}=J_{{\rm SRH},B}+J_{{\rm SRH},E}+J_{{\rm Aug},B}+J_{{\rm Aug},E}+J_{{\rm rad},B}+J_{{\rm rad},E}+J_{\rm BS} \tag{3}$$

and the extra labels E and B are used to indicate on which (emitter or base) side of the SCR the corresponding current is calculated.

In calculating J_B, we neglect the electron current injected from the base into the emitter because the device under study in this report has a $Al_{0.4}Ga_{0.6}As$/GaAs emitter-base junction for which the conduction band discontinuity is equal

[a]Electronic mail: mcahay@planck.ececs.uc.edu

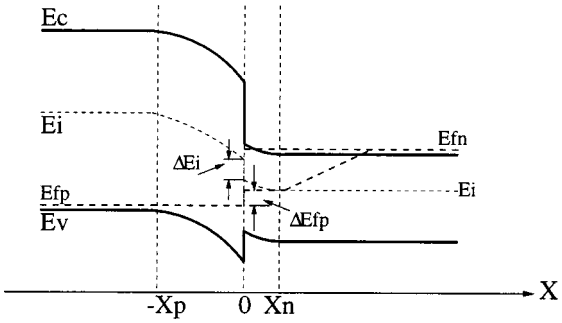

FIG. 1. Schematic energy band diagram illustrating the electron and hole quasi-Fermi level variation across the emitter-base heterojunction and base of a *Pnp* heterojunction bipolar transistor.

to 374 meV, which is large enough to limit to a negligible value the electron current density injected from the base into the emitter.

This article is organized as follows. In Sec. II, we outline the current balancing approach to calculate self-consistently the amount of hole quasi-Fermi level splitting at the emitter-base heterojunction. The latter is then used to determine the various components of the recombination currents affecting hole transport through quasi-neutral base and emitter-base space-charge region. Section III describes an application of our theory to the calculation of the dc current gain as a function of collector current density for a *Pnp* HBT recently reported by Slater *et al.*[19] Section IV contains our conclusions.

II. APPROACH

We consider a typical single heterojunction AlGaAs/GaAs *Pnp* HBT with the structural parameters listed in Table I. For simplicity, the permittivities, effective masses, and effective density of states are assumed to be constant throughout the entire device. Under this approximation, closed form expressions for the recombination currents can be derived if we adopt the linearization procedure of Choo[20] for the electrostatic potential across the emitter-base space-charge region.[16] The results for the Shockley–Read–Hall, Auger, and radiative recombination currents on either side of the emitter-base junction are given in the appendix.

Assuming a SRH recombination process with one type of trap located in the middle of the energy bandgap, the (intrinsic base) surface recombination current at the emitter-base junction can be approximated as:[21]

$$J_{\mathrm{BS}}=\frac{q\sigma v_p}{2}N_{tI}n_{iE}e^{qV_{\mathrm{EB}}/2kT}, \tag{4}$$

TABLE I. *Pnp* HBT structure.

Layer	Material	Thickness (Å)	Doping (cm^{-3})
p^+ (Emitter cap)	GaAs	3500	1×10^{20}
p^+ (Grading)	GaAs/$Al_{0.4}Ga_{0.6}As$	250	1×10^{19}
p (Emitter)	$Al_{0.4}Ga_{0.6}As$	300	1×10^{18}
n^+ (Base)	GaAs	325	7×10^{18}
p (Collector)	GaAs	2300	7×10^{16}
p^+ (Subcollector)	GaAs	5000	7×10^{19}

where k is Boltzmann's constant, T the temperature of the device (assumed to be room temperature), V_{EB} is the emitter-base bias, n_{iE} is the emitter intrinsic carrier concentration, N_{tI} is the heterointerface trap density, $v_p=\sqrt{8kT/\pi m_h^*}$, where m_h^* is the hole density of states effective mass and σ is the surface trap capture cross section.[22]

To calculate the thermionic-tunneling current across the emitter-base junction, we use the conventional expression[23]

$$J_{\mathrm{ThT}}=q\gamma v e^{-\Delta E_p/kT}\left[\frac{n_{iB}^2}{N_D}(e^{qV_{\mathrm{EB}}/kT}-1)-\hat{p}(0)\right], \tag{5}$$

where n_{iB} is the intrinsic carrier concentration in the base region, v is the hole thermal velocity ($\sqrt{kT/2\pi m_h^*}$), and ΔE_v is the valence band discontinuity at the emitter-base junction.

In Eq. (5), $\hat{p}(0)$ is the excess hole concentration in the quasi-neutral base at the edge of the emitter-base space-charge region

$$\hat{p}(0)=\frac{n_{iB}^2}{N_D}[e^{(qV_{\mathrm{EB}}-\Delta E_{fp})/kT}-1]. \tag{6}$$

Furthermore, we have

$$\Delta E_p=\Delta E_v-(1-N_{\mathrm{rat}})(V_{\mathrm{bi}}-V_{\mathrm{EB}}), \tag{7}$$

where $N_{\mathrm{rat}}=N_D/(N_A+N_D)$, N_A and N_D being the uniform doping concentrations in the emitter and base, respectively, and V_{bi} is the emitter-base junction built-in potential.

Typically, for *Npn* HBTs, the tunneling factor γ in Eq. (5) is first computed in the WKB approximation[23] and then cast into a more tractable analytical expression by curve fitting[16] in order to solve Eq. (5) for ΔE_{fp}. Hereafter, we go beyond the WKB approximation and first calculate the hole tunneling current flowing from emitter to base for both heavy and light holes starting with a 4×4 Luttinger–Kohn formalism.[24,25] This formalism includes the non-negligible effects of band mixing between heavy and light holes during tunneling through the emitter-base junction.[24] Then, Eq. (5) is used as a fit because of its simple analytical form to the more rigorous tunneling current including the effects of band mixing. For the specific structure considered in this article,[19] the resulting bias dependence of the tunneling factor γ is found to be[25]

$$\gamma=\frac{0.4383}{e^{q(V_{\mathrm{EB}}-V_{\mathrm{bi}})/3.571kT}+0.00344}. \tag{8}$$

Using the boundary condition (6) and using $\hat{p}(W_{pb})=0$ for the case of a single heterojunction operating in the forward active mode (where W_{pb} is the quasi-neutral base thickness), the neutral-base (J_{NB}) and collector (J_C) currents can be derived using the standard low level injection solution of the continuity equation:[16]

$$J_{\mathrm{NB}}=\frac{qD_p n_{i,B}^2}{N_D L_{pb}}\frac{\cosh(W_{nb}/L_{pb})-1}{\sinh(W_{nb}/L_{pb})}[e^{(qV_{\mathrm{EB}}-\Delta E_{fp})/kT}-1] \tag{9}$$

and

TABLE II. Material and device parameters used in the calculation of the various components of recombination currents.

Emitter ($Al_{0.4}Ga_{0.6}As$	Base (GaAs)
$N_A(cm^{-3})=1.0\times10^{18}$	$N_D(cm^{-3})=7.0\times10^{18}$
$\tau_{n0,p}(ns)=1.0$	$\tau_{n0,n}(ns)=1.0$
$\tau_{p0,p}(ns)=1.0$	$\tau_{p0,n}(ns)=1.0$
$A_{n,p}(cm^6\,s^{-1})=5.8\times10^{-32}$	$A_{n,n}(cm^6\,s^{-1})=1.93\times10^{-31}$
$A_{p,p}(cm^6\,s^{-1})=8.85\times10^{-31}$	$A_{p,n}(cm^6\,s^{-1})=1.12\times10^{-30}$
$B_p(cm^3\,s^{-1})=1.20\times10^{-10}$	$B_n(cm^3\,s^{-1})=7.82\times10^{-11}$

$$J_C=\frac{qD_pn_{i,B}^2}{N_DL_{pb}}\cosh\left(\frac{W_{nb}}{L_{pb}}\right)[e^{(qV_{EB}-\Delta E_{fp})/kT}-1], \qquad (10)$$

where D_p, $L_{pb}(=\sqrt{D_p\tau_{pb}})$, and τ_{pb} are the effective hole diffusion coefficient, diffusion length, and recombination lifetime in the base, respectively.

Next, we apply the theory outlined above to the calculation of the bias dependence of the dc current gain $\beta=J_C/J_B$ for an AlGaAs/GaAs Pnp HBT recently reported by Slater *et al.*[19] To illustrate the importance of the space-charge recombination currents in the space-charge region, we compare the results for β with and without the J_{SCR} term in Eq. (2).

III. RESULTS

The epitaxial layer structure of the Pnp AlGaAs/GaAs HBT considered here is shown in Table I. This structure was investigated experimentally by Slater *et al.*[19] The structure incorporates a graded layer of $Al_xGa_{1-x}As$ ($x=0.0$ to $x=0.4$) between a p-type $Al_{0.4}Ga_{0.6}As$ emitter layer and the highly doped (p^+) GaAs contact layer. The cap and graded layers are used to make a low contact resistance electrical contact to the emitter layer. The material parameters (electron affinities, Auger, and radiative recombination coefficients, minority carrier recombination lifetimes, surface trap carrier cross section) needed to calculate the various recombination currents listed in the appendix are given in Table II.[16,26,27]

First, the valence band energy profile across the emitter-base junction was calculated as a function of the applied emitter-base bias.[28] Next, the hole current flowing from emitter to base was calculated starting from 4×4 Luttinger–Kohn Hamiltonian to include the effects of band mixing between light and heavy holes during tunneling.[24,25] After fitting the results of this approach to the first term on the right-hand side of Eq. (5), we obtained the bias dependence of the tunneling factor γ given in Eq. (8). Figure 2 shows a plot of the bias dependence of the tunneling factor γ. The importance of tunneling is readily apparent in Fig. 2. In a thermionic model of the emitter current, the factor gamma is strictly equal to unity for all biases. A factor gamma larger than unity indicates the importance of tunneling in enhancing the hole emitter current flowing from left to right.

The current balancing Eq. (1) can then be used to determine the hole quasi-Fermi level splitting ΔE_{fp} as a function of applied emitter-base bias V_{EB}. The results are plotted in Fig. 3. This figure indicates that ΔE_{fp} varies from about $2kT$ to $12kT$, while the bias V_{EB} increases from 1.2 to 1.8 V. The latter is slightly below the value of the built-in potential V_{bi} (1.82 eV) calculated using Eq. (A11) in the appendix.

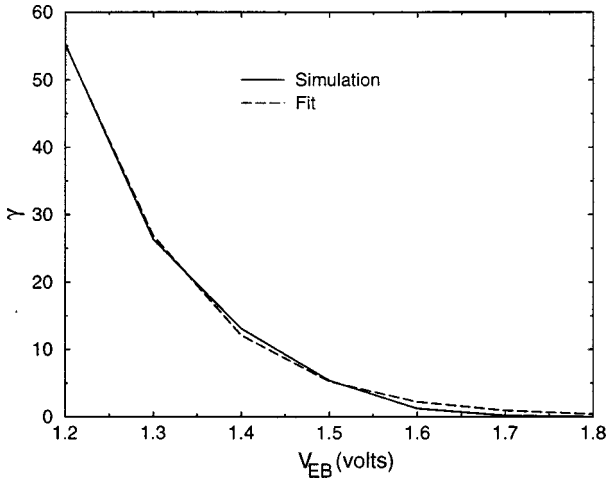

FIG. 2. Full line shows the bias dependence of the tunneling factor γ calculated from a calculation of the collector current density starting from the 4×4 Luttinger–Kohn Hamiltonian (see Refs. 24, 25). The dashed line is a fit to the full line using the analytical expression (see Eq. 8).

Figure 4 is a plot of the collector current density J_C given by Eq. (10) as a function of applied bias. The squares represents the experimental values extracted from Fig. 1(b) in Ref. 19 for a 2×4 μm^2 emitter device. The numerical values are in fairly good agreement with the experimental values considering that we did not include the effects of the series resistance due to the graded AlGaAs layer, cap layer, and emitter contact resistance in our calculations. Including the additional voltage drop across the layers would shift our theoretical results at high bias to the right in Fig. 4 bringing it in closer agreement with the experimental data.

Figure 5 is a plot of the calculated dc current gain versus collector current density. The squares represents the experimental data. The full (dashed) lines are the results obtained

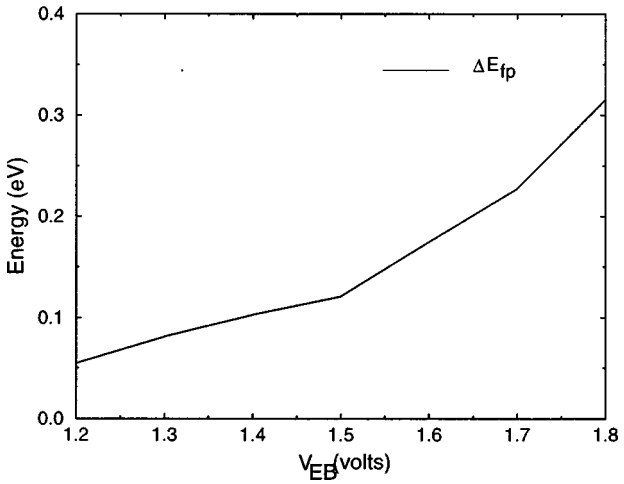

FIG. 3. Bias dependence of the hole quasi-Fermi level splitting at the emitter-base junction of the Pnp HBT with the layer and material parameters listed in Tables I and II.

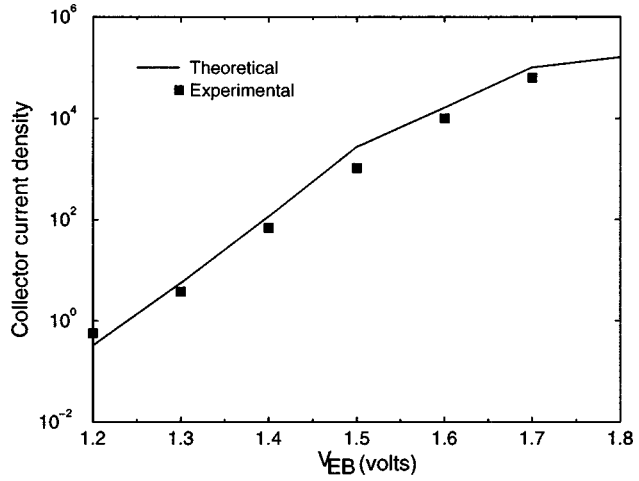

FIG. 4. Comparison between the theoretical (full line) and experimental (squares) collector current density variation with emitter-base bias for the *Pnp* HBT structure with the layer and material parameters listed in Tables I and II (see Ref. 19). The collector current density is in A/cm^2

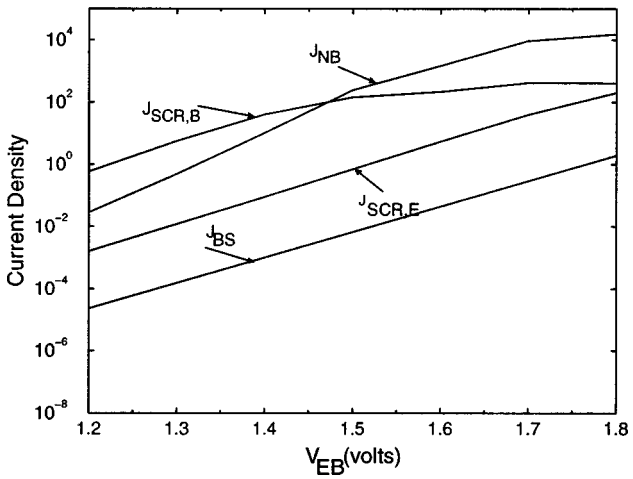

FIG. 6. Bias dependence of the SCR current on the emitter ($J_{SRC,E}$) and base ($J_{SRC,B}$) sides of the SCR, the quasi-neutral-base recombination current (J_{NB}), and the intrinsic base surface recombination current (J_{BS}). The current densities are in A/cm^2

while including (neglecting) the various contributions to the recombination currents in the space-charge region. In both cases, recombination in the quasi-neutral base was taken into account. The agreement between the experiment and theory is quite good with a predicted maximum common emitter dc gain of 10 at $J_C = 10^5$ A/cm^2 compared to a maximum value of 11 measured for $J_C = 2 \times 10^4$ A/cm^2.

Quite noticeable in Fig. 5 is the effects of the space-charge region recombination currents on the dc current gain for low J_C values (1–100 A/cm^2). In this range, the dc current gain is about one order of magnitude below its value calculated while neglecting recombination currents in the space-charge region. To identify the leading contribution in the space-charge region, we plot in Fig. 6 the recombination current components $J_{SCR,E}$, $J_{SCR,B}$, J_{NB}, and J_{BS} as a function of applied emitter-base bias. This figure indicates the leading contribution to the base current is $J_{SRH,B}$ at low bias and J_{NB} for biases closer to the built-in potential (1.82 eV). This figure also shows that the contribution of the surface recombination current is negligible for all biases.

Finally, Fig. 7 shows a plot of the bias dependence of $J_{SRH,B}$, $J_{Aug,B}$, and $J_{rad,B}$, indicating that the SRH mechanism is the leading recombination current over most of the bias range. The radiative recombination process is comparable in size only for voltages approaching the built-in potential.

IV. CONCLUSIONS

Using a current balancing approach between the thermionic-tunneling current across the emitter-base junction, the collector current, and the various recombination current components in the emitter-base space-charge region and the quasi-neutral base, we have determined the amount of hole quasi-Fermi level splitting at the emitter-base junc-

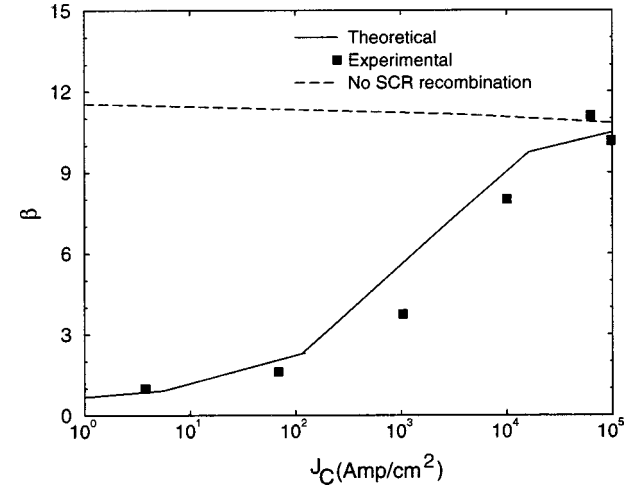

FIG. 5. DC current gain vs collector current density. The full line is the theoretical result and the dashed line is the dc current gain when the space-charge recombination current components are neglected.

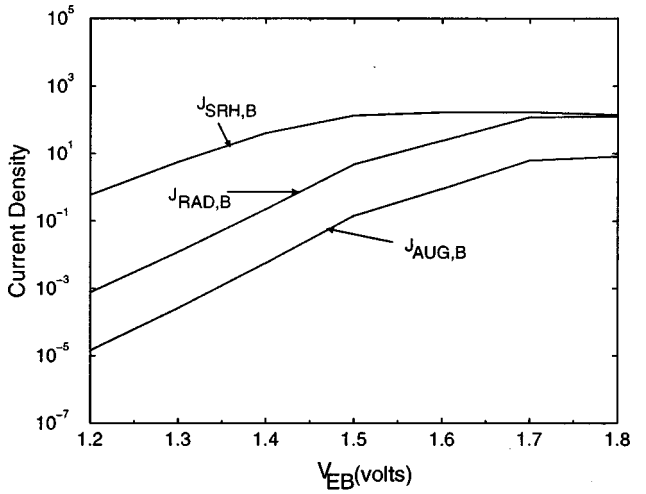

FIG. 7. Bias dependence of the SRH, Auger, and radiative recombination currents on the base side of the SCR. The current densities are in A/cm^2.

tion for a typical AlGaAs/GaAs *Pnp* HBT as a function of the applied bias. This Fermi level splitting has been used to calculate the total base current while including the effects of Shockley–Read–Hall, Auger, radiative, and (intrinsic) base surface recombination in the emitter-base space-charge region. The contribution from the electron current injected from base back into the emitter was neglected in calculating the base current because the conduction band step is large for the particular *Pnp* device investigated here.[19] A novelty of our approach is that the hole current density was calculated using a 4×4 Luttinger–Kohn Hamiltonian including the effects of heavy- and light-hole band mixing during tunneling.[24,25]

Very good agreement between theory and experiment is found for the dc current gain dependence on the collector current density when the SCR recombination currents were included in the analysis. At low emitter-base bias, the leading contribution to the base current is found to be the Shockley–Read–Hall recombination current on the base side of the SCR. At biases approaching the built-in potential, the recombination current in the quasi-neutral base is found to be equally important. The model described here should be quite useful to device engineers for the design of *Pnp* HBTs prior to actual device fabrication.

ACKNOWLEDGMENT

This work was supported by the National Science Foundation under Grant No. ECS-9525942.

APPENDIX A

In this appendix, we give the explicit analytical expressions for the SRH, Auger, and radiative recombination currents on either side of the emitter-base space-charge region. These expressions were derived following the approach of Searles and Pulfrey for *Npn* HBTs.[17]

The SRH recombination current density on the emitter side of the SRC is given by

$$J_{\mathrm{SRH},E}=\frac{2qn_{iE}W_{\mathrm{BE}}}{\tau_E\Theta}\sinh\left(\frac{qV_{\mathrm{EB}}}{2kT}\right)\operatorname{atan}\left(\frac{Z_p-Z_{\mathrm{op}}}{1+Z_pZ_{\mathrm{op}}}\right), \quad \text{(A1)}$$

where

$$Z_p=\left(\frac{N_A}{n_{iE}}\right)\sqrt{\frac{\tau_{p0,E}}{\tau_{n0,E}}}\,e^{-qV_{\mathrm{EB}}/2kT}, \quad \text{(A2)}$$

and

$$Z_{\mathrm{op}}=Z_pe^{-\Theta N_{\mathrm{rat}}}. \quad \text{(A3)}$$

In Eq. (A1), $\Theta=[q(V_{bi}-V_{\mathrm{EB}})]/kT$ and n_{iE} is the intrinsic carrier concentration in the emitter region. Furthermore, $\tau_E=\sqrt{\tau_{p0,E}\tau_{n0,E}}$, where $(\tau_{p0,E},\tau_{n0,E})$ are the hole and electron minority carrier lifetimes in the emitter side of the space-charge region.

The SRH recombination current density on the base side of the SCR is found to be

$$J_{\mathrm{SRH},B}=\frac{2qn_{iB}W_{\mathrm{BE}}}{\tau_B\Theta}\sinh\left(\frac{qV_{\mathrm{EB}}-\Delta_{E_{fp}}}{2kT}\right)\operatorname{atan}\left(\frac{Z_{\mathrm{on}}-Z_n}{1+Z_nZ_{\mathrm{on}}}\right), \quad \text{(A4)}$$

with

$$Z_{\mathrm{on}}=\left(\frac{N_A}{n_{iE}}\right)\sqrt{\frac{\tau_{p0,B}}{\tau_{n0,B}}}\,e^{(-2qN_{\mathrm{rat}}(V_{bi}-V_{\mathrm{EB}})+2\Delta E_i-qV_{\mathrm{EB}}-\Delta E_{fp})/2kT}, \quad \text{(A5)}$$

and

$$Z_n=Z_{\mathrm{on}}e^{-\Theta(1-N_{\mathrm{rat}})}. \quad \text{(A6)}$$

where $\tau_B=\sqrt{\tau_{p0,B}\tau_{n0,B}}$, $(\tau_{p0,B},\tau_{n0,B})$ being the hole and electron minority carrier lifetimes in the base side of the space-charge region.

For the Auger recombination currents, we find

$$J_{\mathrm{Aug},E}=\frac{2qn_{iE}^3}{\tau_E}\frac{W_{\mathrm{BE}}}{\Theta}\frac{(Z_p-Z_{\mathrm{op}})}{Z_pZ_{\mathrm{op}}}e^{qV_{\mathrm{EB}}/kT}\sinh\left(\frac{qV_{\mathrm{EB}}}{2kT}\right)\times(A_{n,E}\tau_{n0,E}Z_pZ_{\mathrm{op}}+A_{p,E}\tau_{p0,E}), \quad \text{(A7)}$$

and

$$J_{\mathrm{Aug},B}=\frac{2qn_{iB}^3}{\tau_B}\frac{W_{\mathrm{BE}}}{\Theta}\frac{(Z_{\mathrm{on}}-Z_n)}{Z_nZ_{\mathrm{on}}}e^{(qV_{\mathrm{EB}}-\Delta E_{fp})/kT}\times\sinh\left(\frac{qV_{\mathrm{EB}}-\Delta E_{fp}}{2kT}\right)(A_{n,B}\tau_{n0,B}Z_nZ_{\mathrm{on}}+A_{p,B}\tau_{p0,B}), \quad \text{(A8)}$$

where $(A_{n,E},A_{p,E})$ and $(A_{n,B},A_{p,B})$ are the electron and hole Auger recombination coefficients on the emitter and base sides of the SCR, respectively.[26]

Finally, the radiative recombination currents are given by

$$J_{\mathrm{rad},E}=qB_pn_{iE}^2W_{\mathrm{BE}}N_{\mathrm{rat}}(e^{qV_{\mathrm{EB}}/kT}-1) \quad \text{(A9)}$$

and

$$J_{\mathrm{rad},B}=qB_nn_{iB}^2W_{\mathrm{BE}}(1-N_{\mathrm{rat}})(e^{qV_{\mathrm{EB}}-\Delta E_{fp})/kT}-1), \quad \text{(A10)}$$

where B_p and B_n are the radiative recombination coefficients on the emitter and base sides of the SCR, respectively.

In all the expressions above, the emitter-base junction built-in potential V_{bi} and the intrinsic Fermi level discontinuity at the emitter-base heterojunction are given by[17]

$$V_{\mathrm{bi}}=\frac{kT}{q}\ln\left(\frac{N_AN_D}{n_{iE}n_{iB}}\right)+\Delta E_i, \quad \text{(A11)}$$

$$\Delta E_i=\frac{kT}{q}\ln\left(\frac{n_{iE}}{n_{iB}}\right)+(\chi_B-\chi_E), \quad \text{(A12)}$$

where χ_B and χ_E are the electron affinities of the base and emitter regions, respectively. For the particular *Pnp* HBT investigated in this work,[18] we have $V_{\mathrm{bi}}=1.82\,\mathrm{V}$, $\Delta E_i=217\,\mathrm{meV}$, $\chi_B=4.07\,\mathrm{eV}$, and $\chi_E=3.63\,\mathrm{eV}$.[25]

[1] P. M. Enquist, D. B. Slater, and J. W. Stuart, IEEE Electron Device Lett. **13**, 180 (1992).
[2] D. B. Slater, P. M. Enquist, F. E. Najjar, M. Y. Chen, and J. A. Hutchby, Proc. SPIE **1288**, 90 (1990).
[3] D. B. Slater, P. M. Enquist, F. E. Najjar, M. Y. Chen, and J. A. Hutchby, IEEE Electron Device Lett. **11**, 146 (1990).
[4] F. E. Najjar, P. M. Enquist, D. B. Slater, and M. Y. Chen, Electron. Lett. **25**, 1405 (1989).
[5] D. B. Slater, P. M. Enquist, M. Y. Chen, J. A. Hutchby, A. S. Morris and R. J. Trew, IEEE Electron Device Lett. **12**, 382 (1991).
[6] T. De Lyon, H. C. Casey, P. M. Enquist, and J. A. Hutchby, IEEE Trans. Electron Devices **35**, 1389 (1988).
[7] T. De Lyon, H. C. Casey, P. M. Enquist, J. A. Hutchby, and A. J. Spring-Thorpe, Appl. Phys. Lett. **54**, 641 (1989).
[8] D. G. Hill, W. S. Lee, T. Ma, and J. S. Harris, IEEE Electron Device Lett. **11**, 425 (1990).
[9] D. G. Hill, W. S. Lee, T. Ma, and J. S. Harris, Electron. Lett. **25**, 993 (1989).
[10] W. Liu, D. Hill, D. Costa, and J. S. Harris, IEEE Microwave Guid. Wave Lett. **2**, 331 (1992).
[11] W. Liu, D. Hill, D. Costa, and J. S. Harris, Electron. Lett. **26**, 2001 (1990).
[12] J. A. Hutchby, IEEE Electron Device Lett. **7**, 108 (1986).
[13] D. A. Sunderland and P. D. Dapkus, IEEE Trans. Electron Devices **34**, 367 (1987).
[14] J. S. Yuan, Solid-State Electron. **34**, 1347 (1991).
[15] J. J. Liou, J. Appl. Phys. **69**, 3328 (1991).
[16] S. Searles and D. L. Pulfrey, IEEE Trans. Electron Devices **41**, 476 (1994).
[17] S. S. Perlman and D. L. Feucht, Solid-State Electron. **7**, 911 (1964).
[18] S. Datta, K. P. Roenker, and M. Cahay, J. Appl. Phys. **85**, 1949 (1999).
[19] D. B. Slater, P. M. Enquist, J. A. Hutchby, A. S. Morris, and R. J. Trew, IEEE Electron Device Lett. **15**, 91 (1994).
[20] C. C. Choo, Solid-State Electron. **11**, 1069 (1968).
[21] J. J. Liou and J. S. Yuan, Solid-State Electron. **35**, 805 (1992).
[22] E. S. Yang, *Microelectronic Devices* (McGraw–Hill, New York, 1988).
[23] A. A. Grindberg, M. S. Shur, R. J. Fisher, and H. Morkoc, IEEE Trans. Electron Devices **31**, 1758 (1984).
[24] T. Kumar, M. Cahay, and K. Roenker, Phys. Rev. B **56**, 4836 (1997).
[25] S. Ekbote, M. Cahay, and K. Roenker (unpublished).
[26] S. Adachi, *GaAs and Related Materials* (World Scientific, Singapore, 1994), p. 546.
[27] M. Takeshima, J. Appl. Phys. **58**, 3846 (1985).
[28] We used the program FISH1D (version 2.1) released by Purdue University.